Brian Homeijer
R&D Engineer
Technology Development Organization,
Image and Printing Group,
HP, Corvallis, OR 97330
e-mail: brian.homeijer@hp.com

Benjamin A. Griffin
Postdoctoral Associate

Matthew D. Williams
Graduate Research Assistant

Bhavani V. Sankar
Ebaugh Professor

Mark Sheplak[1]
Professor
e-mail: sheplak@ufl.edu

Interdisciplinary Microsystems Group,
Department of Mech. & Aero. Eng.,
Univ. of Florida,
Gainesville, FL 32611-6250

Composite Circular Plates With Residual Tensile Stress Undergoing Large Deflections

Many micromachined electroacoustic devices use thin plates in conjunction with electrical components to measure acoustic signals. Composite layers are needed for electrical passivation, moisture barriers, etc. The layers often contain residual stresses introduced during the fabrication process. Accurate models of the composite plate mechanics are crucial for predicting and optimizing device performance. In this paper, the von Kármán plate theory is implemented for a transversely isotropic, axisymmetric plate with in-plane tensile stress and uniform transverse pressure loading. A numerical solution of the coupled force-displacement nonlinear differential equations is found using an iterative technique. The results are verified using finite element analysis. This paper contains a study of the effects of tensile residual stresses on the displacement field and examines the transition between linear and nonlinear behavior. The results demonstrate that stress stiffening in the composite plate delays the onset of nonlinear deflections and decreases the mechanical sensitivity. In addition, under high stress the plate behavior transitions to that of a membrane and becomes insensitive to the composite nature of the plate. The results suggest a tradeoff between mechanical sensitivity and linearity.
[DOI: 10.1115/1.4005534]

1 Introduction

Many microelectromechanical systems (MEMS) based electroacoustic devices, such as microphones, utilize composite plates [1–3]. The plate's mechanical response to acoustic pressure oscillations is important in determining the sensitivity, bandwidth, and dynamic range of the electroacoustic device. The mechanical sensitivity of the device is dependent upon the plate compliance. The bandwidth is the frequency range over which the sensitivity is approximately constant. The resonance of the diaphragm determines the upper limit of the bandwidth. The dynamic range is the difference between the minimum detectable pressure and the maximum pressure where the sensitivity is independent of applied pressure.

In a piezoresistive MEMS microphone; for example, a silicon dioxide layer thermally grown on a silicon substrate provides electrical passivation and a silicon nitride layer deposited on top of the oxide serves as a hydrophobic barrier. The thermally grown oxide contains compressive stress and the deposited nitride layer can be tailored to be in tension or compression. A compressive stress increases the plate's sensitivity to pressure and lowers the pressure at which the onset of nonlinear deflection occurs [3]. A sufficiently large compressive stress buckles the device. In contrast, a tensile stress lowers the sensitivity of the device while increasing the upper limit of the dynamic range [4]. Due to the significant impact of residual stresses on device performance, they must be incorporated into the model used in the design process.

Optimization has been shown to be an important tool in electroacoustic device design [5]. The performance tradeoff between the device sensitivity and noise floor suggests that the minimum detectable pressure is an appropriate objective function in microphone design optimization [5]. Performance, fabrication, and model accuracy constraints are required in the optimization. Two performance constraints are the bandwidth and the upper limit of the dynamic range. Linear plate theory is used to determine the mechanical sensitivity and bandwidth, but a nonlinear plate model is needed to predict the upper limit of the dynamic range.

The large deflection theory for isotropic, clamped plates with zero in-plane load is discussed in Timoshenko and Woinowsky-Krieger [6]. Sheplak and Dugundji [4] extended this work to nonlinear deflections of isotropic plates with tensile in-plane loading. The current effort builds upon the previous work by incorporating composite layers in the diaphragms. The structure analyzed is representative of a MEMS microphone. The plate is composed of a silicon-silicon dioxide-silicon nitride composite with material parameters shown in Table 1. This analysis, however, can be tailored for any number of composite layers, residual stresses, and material properties.

The derivation presented considers an axisymmetric plate and assumes transversely isotropic layers. The approximation of silicon as mechanically isotropic is common for MEMS structures due to its low degree of anisotropy [7,8]. The straindisplacement relationship implemented includes the von Kármán strains to accurately predict large deflections. Residual stresses are assumed to be uniform in each plate layer. The derivation results in two nonlinear, coupled, ordinary differential equations governing transverse deflection and the radial force resultant. The equations are nondimensionalized and solved using an iterative finite difference method. Results are reported for different combinations of nondimensional parameters that capture the composite lay-up and

Table 1 Material and geometric parameters

Parameter	Si	SiO_2	Si_xN_y
Layer thickness[a] (μm)	10	0.3	0.3
Young's modulus (GPa)	170	73	384
Poisson's ratio	0.27	0.17	0.24

[a]The diaphragm radius is $a = 1.47$ mm with a total diaphragm thickness $h = 10.6\ \mu$m.

[1]Corresponding author.

Manuscript received January 24, 2011; final manuscript received April 28, 2011; accepted manuscript posted January 25, 2012; published online February 13, 2012. Assoc. Editor: Anthony Waas.

plate geometry. The impact of in-plane tension on mechanical sensitivity and the onset of nonlinearity are discussed.

2 Basic Equations

Consider the cross section of an axisymmetric, composite plate shown in Fig. 1. A constant tensile in-plane stress, σ_0, is assumed to exist in one or more of the layers. A uniform transverse load, p, is applied on the surface. Although only three layers are shown, the solution methodology is applicable to an arbitrary number of layers. The equilibrium equations of the axisymmetric plate are [9]:

$$\frac{dN_r}{dr} + \frac{N_r - N_\theta}{r} = 0 \tag{1}$$

$$\frac{d}{dr}\left(r\frac{dw}{dr}N_r\right) + rp + \frac{d}{dr}(rQ_r) = 0 \tag{2}$$

and

$$\frac{dM_r}{dr} + \frac{M_r - M_\theta}{r} = Q_r \tag{3}$$

where N_r and N_θ are the radial and tangential in-plane force resultants, M_r and M_θ are the radial and tangential bending moment resultants, Q_r is the shear force resultant, and w is the deflection in the positive z direction.

Assuming an axisymmetric plate, the radial and tangential Green strain tensor simplified for small strains but moderate rotations in terms of displacement fields, u_r and u_z, are [6]

$$\begin{Bmatrix} \varepsilon_r \\ \varepsilon_\theta \end{Bmatrix} = \begin{Bmatrix} \dfrac{\partial u_r}{\partial r} + \dfrac{1}{2}\left(\dfrac{\partial u_z}{\partial r}\right)^2 \\ \dfrac{u_r}{r} \end{Bmatrix} \tag{4}$$

The Kirchhoff hypothesis yields the displacement field for a thin circular plate under uniform transverse loading is [9]

$$u_z(r,z) = w(r) \tag{5}$$

and

$$u_r(r,z) = u_0(r) - z\frac{\partial w(r)}{\partial r} \tag{6}$$

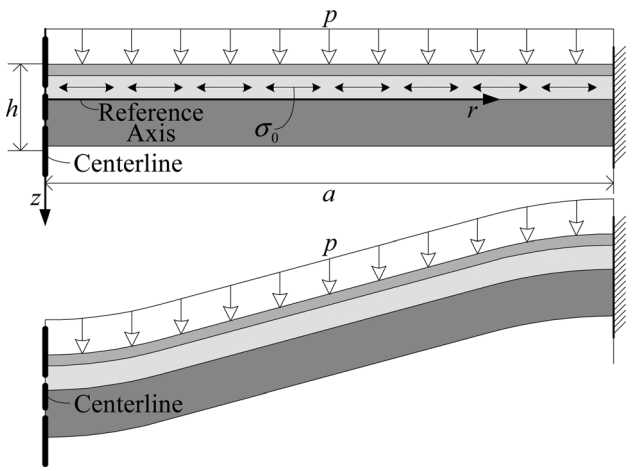

Fig. 1 Cross section of an axisymmetric, composite plate with in-plane stress in the second layer

where $u_0(r)$ is the radial and w (r) is the vertical displacement of points on the reference surface $(z=0)$ shown in Fig. 1. Substituting the displacement fields into Eq. (4), the strain relationships become [10]

$$\begin{Bmatrix} \varepsilon_r \\ \varepsilon_\theta \end{Bmatrix} = \begin{Bmatrix} \varepsilon_r^0 \\ \varepsilon_\theta^0 \end{Bmatrix} + z\begin{Bmatrix} \kappa_r \\ \kappa_\theta \end{Bmatrix} \tag{7}$$

where the reference plane strains are

$$\begin{Bmatrix} \varepsilon_r^0 \\ \varepsilon_\theta^0 \end{Bmatrix} = \begin{Bmatrix} \dfrac{du_0}{dr} + \dfrac{1}{2}\left(\dfrac{dw}{dr}\right)^2 \\ \dfrac{u_0}{r} \end{Bmatrix} \tag{8}$$

and the curvatures are

$$\begin{Bmatrix} \kappa_r \\ \kappa_\theta \end{Bmatrix} = \begin{Bmatrix} -\dfrac{d^2w}{dr^2} \\ -\dfrac{1}{r}\dfrac{dw}{dr} \end{Bmatrix} \tag{9}$$

The plate is assumed to be transversely isotropic. The constitutive relationship for an axisymmetric plate including the residual stress is

$$\begin{Bmatrix} \sigma_r^n \\ \sigma_\theta^n \end{Bmatrix} = \begin{Bmatrix} \sigma_0^n \\ \sigma_0^n \end{Bmatrix} + [Q_n]\begin{Bmatrix} \varepsilon_r^0 \\ \varepsilon_\theta^0 \end{Bmatrix} + z[Q_n]\begin{Bmatrix} \kappa_r \\ \kappa_\theta \end{Bmatrix} \tag{10}$$

where σ_0^n is the residual stress in the nth layer and $[Q_n]$ is the stiffness matrix of the nth layer,

$$[Q_n] = \frac{E_n}{1-\nu_n^2}\begin{bmatrix} 1 & \nu_n \\ \nu_n & 1 \end{bmatrix} \tag{11}$$

Here, E_n and ν_n are the modulus of elasticity and Poisson's ratio in the plane of the plate, respectively. The force and moment resultants are found by taking the zeroth and first moments of the stresses through the thickness of the plate, respectively, and are

$$\begin{Bmatrix} N_r \\ N_\theta \end{Bmatrix} = \int_{z_B}^{z_T}\begin{Bmatrix} \sigma_r^n \\ \sigma_\theta^n \end{Bmatrix}dz = \begin{Bmatrix} N_0 \\ N_0 \end{Bmatrix} + [A]\begin{Bmatrix} \varepsilon_r^0 \\ \varepsilon_\theta^0 \end{Bmatrix} + [B]\begin{Bmatrix} \kappa_r \\ \kappa_\theta \end{Bmatrix} \tag{12}$$

and

$$\begin{Bmatrix} M_r \\ M_\theta \end{Bmatrix} = \int_{z_B}^{z_T}\begin{Bmatrix} \sigma_r^n \\ \sigma_\theta^n \end{Bmatrix}zdz = \begin{Bmatrix} M_0 \\ M_0 \end{Bmatrix} + [B]\begin{Bmatrix} \varepsilon_r^0 \\ \varepsilon_\theta^0 \end{Bmatrix} + [D]\begin{Bmatrix} \kappa_r \\ \kappa_\theta \end{Bmatrix} \tag{13}$$

where z_T and z_B are coordinates identifying the top and bottom of the plate. The $[A]$, $[B]$, and $[D]$ matrixes are the extensional, flexural-extensional coupling, and flexural stiffness matrixes, respectively, and are defined as [10],

$$\begin{Bmatrix} [A] \\ [B] \\ [D] \end{Bmatrix} = \int_{z_B}^{z_T}[Q_n]\begin{Bmatrix} 1 \\ z \\ z^2 \end{Bmatrix}dz \tag{14}$$

Equations (1)–(13) are combined to form a differential equation in terms of deflection slope and radial force resultant. First, Eq. (2) is integrated,

$$\frac{dw}{dr}N_r + \frac{r}{2}p + Q_r = 0 \tag{15}$$

and combined with Eq. (3) to yield

$$\frac{dM_r}{dr}+\frac{M_r-M_\theta}{r}+\frac{dw}{dr}N_r+\frac{r}{2}p=0 \tag{16}$$

Substituting Eq. (13) into Eq. (16) results in

$$\frac{d^3w}{dr^3}+\frac{d}{dr}\left(\frac{1}{r}\frac{dw}{dr}\right)-\frac{N_0}{D^*}\frac{dw}{dr}=\frac{1}{D^*}\frac{dw}{dr}\left[B_{12}^*\frac{1}{2}\frac{1}{r}\frac{dw}{dr}+\tilde{N}_r\right]+r\frac{p}{2D^*} \tag{17}$$

where $\tilde{N}_r=N_r-N_0$, $B_{12}^*=B_{11}(A_{12}/A_{11})-B_{12}$, and $D*=D_{11}-\left(B_{11}^2/A_{11}\right)$. By introducing the transverse deflection slope (or approximate rotation angle of the transverse normals), $\phi=-dw/dr$, Eq. (17) becomes

$$\frac{d^2\phi}{dr^2}+\frac{d}{dr}\left(\frac{\phi}{r}\right)-\frac{N_0}{D^*}\phi=\frac{\phi\tilde{N}_r}{D^*}-\frac{B_{12}^*}{2D^*}\frac{\phi^2}{r}-r\frac{p}{2D^*} \tag{18}$$

Equation (18) is a nonlinear differential equation with two unknowns, ϕ and $\tilde{N}_r$. Therefore, another equation with ϕ and $\tilde{N}_r$ as dependent variables is required. The second equation is derived from the strain compatibility equation [6],

$$\varepsilon_r^0=\frac{d(r\varepsilon_\theta^0)}{dr}+\frac{1}{2}\phi^2 \tag{19}$$

Solving Eq. (12) for the radial and tangential strains and substituting into Eq. (19) results in an equation in terms of ϕ and $\tilde{N}_r$,

$$r^2\frac{d^2\tilde{N}_r}{dr^2}+3r\frac{d\tilde{N}_r}{dr}=-B_{12}^*\left(r\frac{d^2\phi}{dr^2}+\frac{d\phi}{dr}-\frac{\phi}{r}\right)-\frac{A_{11}^2-A_{12}^2}{A_{11}}\frac{\phi^2}{2} \tag{20}$$

Equations (18) and (20) form two mixed force and displacement, nonlinear differential equations in dependent variables ϕ and $\tilde{N}_r$. Finally Eq. (12) is substituted into Eq. (1). yielding

$$\frac{d^2u_0}{dr^2}+\frac{1}{r}\frac{du_0}{dr}-\frac{u_0}{r^2}=\frac{B_{11}}{A_{11}}\left(\frac{d^2\phi}{dr^2}+\frac{1}{r}\frac{d\phi}{dr}-\frac{\phi}{r^2}\right)-\left(1-\frac{A_{12}}{A_{11}}\right)\frac{\phi^2}{2r}-\phi\frac{d\phi}{dr} \tag{21}$$

a nonlinear ordinary differential equation for the radial displacements along the reference surface. Equations (18), (20), and (21) are nondimensionalized using the following definitions

$$\xi=\frac{r}{a},\quad \eta=\frac{z}{h},\quad W=\frac{w}{h},\quad \Theta=-\frac{dW}{d\xi}=\frac{a}{h}\phi,\quad U=\frac{u_0}{h},$$
$$S_r^*=\frac{\tilde{N}_r a^2}{D^*},\quad k^*=\sqrt{\frac{N_0a^2}{D^*}},\quad \text{and}\quad P^*=\frac{pa^4}{2hD^*}$$

where a and h are the radius and total thickness of the plate, respectively. The nondimensionalization is similar to that of Sheplak and Dugundji [4]. It is important to note, however, that S_r^*, $k*$, and $P*$ are influenced by the composite nature of the plate through the composite stiffness, $D*$. The resulting nondimensional equations are

$$\frac{d^2\Theta}{d\xi^2}+\frac{1}{\xi}\frac{d\Theta}{d\xi}-\left(k^{*2}+\frac{1}{\xi^2}\right)\Theta=-P^*\xi+S_r^*\Theta-\frac{\Lambda}{2\xi}\Theta^2 \tag{22}$$

$$\xi^2\frac{d^2S_r^*}{d\xi^2}+3\xi\frac{dS_r^*}{d\xi}=-\Lambda\left(\xi\frac{d^2\Theta}{d\xi^2}+\frac{d\Theta}{d\xi}-\frac{\Theta}{\xi}\right)-\frac{X}{2}\Theta^2 \tag{23}$$

and

$$\frac{d^2U}{d\xi^2}+\frac{1}{\xi}\frac{dU}{d\xi}-\frac{U}{\xi^2}=-\varsigma\left(\eta_{na}\left(\frac{d^2\Theta}{d\xi^2}+\frac{1}{\xi}\frac{d\Theta}{d\xi}-\frac{\Theta}{\xi^2}\right)+\Theta\left[\left(1-\frac{A_{12}}{A_{11}}\right)\frac{\Theta}{2\xi}+\frac{d\Theta}{d\xi}\right]\right) \tag{24}$$

where

$$\Lambda=\frac{B_{12}^*h}{D^*},\quad X=\frac{A_{11}^2-A_{12}^2}{A_{11}}\frac{h^2}{D^*},\quad \varsigma=\frac{h}{a}$$

and

$$\eta_{na}=\frac{B_{11}}{A_{11}}\frac{1}{h}$$

The Λ coefficient increases in magnitude as the plate becomes more asymmetric and goes to zero for a symmetric composite. The X coefficient is dependent upon the variation in the material properties of the composite layers. The η_{na} coefficient is the nondimensional distance from the reference axis to the neutral axis. It is important to note that Eq. (22), Eq. (23), and Eq. (24) reduce to the equations of Sheplak and Dugundji [4] for a homogenous plate with $z=0$ at its midplane.

The stresses within the plate Eq. (10) are nondimensionalized as

$$\begin{Bmatrix}\Sigma_r^n\\ \Sigma_\theta^n\end{Bmatrix}=\frac{1}{E_{nd}\varsigma^2}\begin{Bmatrix}\sigma_r^n\\ \sigma_\theta^n\end{Bmatrix} \tag{25}$$

where E_{nd} is the chosen modulus of elasticity for nondimensionalization. The nondimensional stress can be decomposed into residual stress and stress due to transverse loading,

$$\begin{Bmatrix}\Sigma_r^n\\ \Sigma_\theta^n\end{Bmatrix}=\begin{Bmatrix}\Sigma_0^n\\ \Sigma_0^n\end{Bmatrix}+\begin{Bmatrix}\tilde{\Sigma}_r^n\\ \tilde{\Sigma}_\theta^n\end{Bmatrix} \tag{26}$$

where the stress due to loading $(\tilde{\Sigma}^n)$ is

$$\begin{Bmatrix}\tilde{\Sigma}_r^n\\ \tilde{\Sigma}_\theta^n\end{Bmatrix}=\frac{\Pi}{(1-\nu_n^2)}\left(\frac{1}{\varsigma}\begin{Bmatrix}\frac{dU}{d\xi}+\nu_n\frac{U}{\xi}\\ \nu_n\frac{dU}{d\xi}+\frac{U}{\xi}\end{Bmatrix}+\eta\begin{Bmatrix}\frac{d\Theta}{d\xi}+\nu_n\frac{\Theta}{\xi}\\ \nu_n\frac{d\Theta}{d\xi}+\frac{\Theta}{\xi}\end{Bmatrix}\right) \tag{27}$$

and $\Pi=\frac{E_n}{E_{nd}}$.

2.1 Boundary Conditions. The plate is assumed to have clamped boundary conditions such that the slope and radial displacement is zero at the plate's edge,

$$\Theta(\xi=1)=0 \tag{28}$$

and

$$U(\xi=1)=0. \tag{29}$$

The symmetry condition dictates that the deflection slope and radial displacement is zero at the plate's center,

$$\Theta(\xi=0)=0 \tag{30}$$

and

$$U(\xi=0)=0 \tag{31}$$

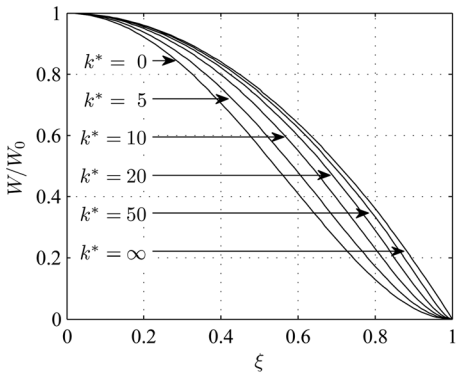

(a) Deflection normalized by center deflection, W_0.

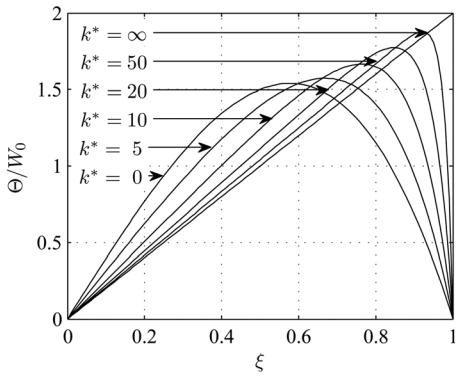

(b) Slope normalized by center deflection, W_0.

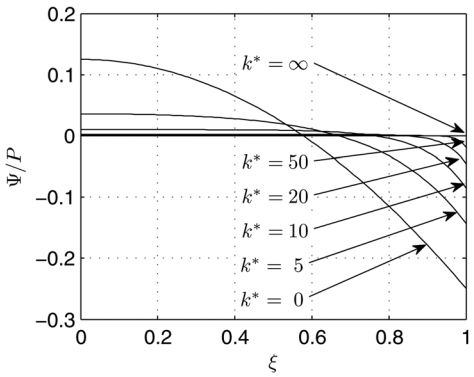

(c) Curvature normalized by P^*.

Fig. 2 Linear nondimensional solution for various *k**

Two boundary conditions on S_r^* are also needed. The symmetry condition also dictates that the radial change in the incremental radial force resultant is zero at the plate's center,

$$\left.\frac{dS_r^*}{d\xi}\right|_{\xi=0} = 0 \tag{32}$$

The second boundary condition on S_r^* is derived from the clamped radial displacement boundary condition, Eq. (29). Combining Eq. (29) with Eqs. (1), (8), and (12), gives the second boundary condition,

$$\left.\frac{dS_r^*}{d\xi}\right|_{\xi=1} + \left(1 - \frac{A_{12}}{A_{11}}\right) S_r^*|_{\xi=1} = -\Lambda \left.\frac{d\Theta}{d\xi}\right|_{\xi=1} \tag{33}$$

The deflection is obtained by integrating the slope Θ and applying a clamped boundary condition on the edge of the plate,

$$W(\xi = 1) = 0 \tag{34}$$

2.2 Linear Theory. For small deflections, the nonlinear terms in Eq. (22) are neglected and the resulting governing equation is uncoupled from S_r^*,

$$\frac{d^2\Theta}{d\xi^2} + \frac{1}{\xi}\frac{d\Theta}{d\xi} - \left(k^{*2} + \frac{1}{\xi^2}\right)\Theta = -P^*\xi \tag{35}$$

The slope, transverse deflection, and curvature solutions are

$$\Theta(\xi) = \frac{P^*}{k^{*2}}\left(\xi - \frac{I_1(k^*\xi)}{I_1(k^*)}\right) \tag{36}$$

$$W(\xi) = \frac{P^*}{k^{*2}}\left\{\frac{(1-\xi^2)}{2} + \frac{1}{k^*}\frac{I_0(k^*)}{I_1(k^*)}\left[\frac{I_0(k^*\xi)}{I_0(k^*)} - 1\right]\right\} \tag{37}$$

and

$$\Psi(\xi) = \frac{P^*}{k^{*2}}\left(1 - \frac{k^* I_0(k^*\xi)}{I_1(k^*)} + \frac{I_1(k^*\xi)}{\xi I_1(k^*)}\right) \tag{38}$$

respectively, where I_0 and I_1 are modified Bessel functions of the first kind and the nondimensional curvature is defined as $\Psi = d\Theta/d\xi$. Neglecting the nonlinear terms in Eq. (24) and substituting in Eq. (36) yields the radial displacement

$$U = \frac{\eta_{na}\varsigma P^*}{k^{*2}}\left(\frac{I_1(k^*\xi)}{I_1(k^*)} - \xi\right) \tag{39}$$

The slope, deflection, and curvature results are plotted in Fig. 2. These results are similar in nature to the isotropic case [4] with the effect of the composite accounted for in k^* and D^*. The linear theory for a composite differs from the isotropic case by having a finite radial displacement. It is easily seen from Eq. (39) that in the limit of a homogenous plate evaluated at the midplane, i.e., $\eta_{na} \to 0$, the radial strain is identically zero. As the tension parameter, k^*, becomes large, the transverse deflection's inflection point (where curvature equals zero) gets closer to the edge of the plate and the deflection slope gradients become severe. This is indicative of an edge zone that develops between the point of maximum deflection slope and the clamped boundary condition at the plate's edge. As the tension parameter increases, this zone becomes smaller and the gradient in the deflection becomes larger. Similar to the isotropic plate case, the extent of this edge zone is estimated by $\Delta\xi \approx 3/k^*$ [4]. In a numerical solution, the edge zone must be

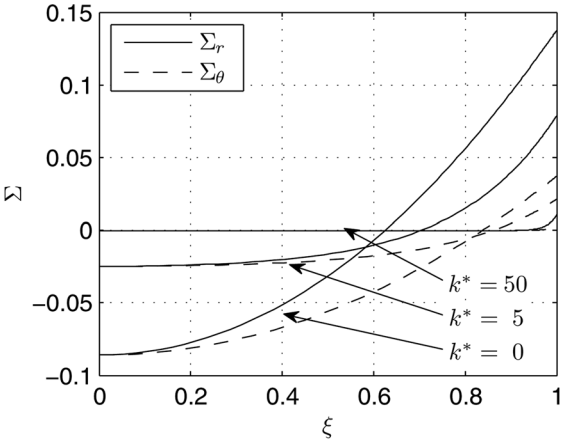

(a) Radial and tangential stress as a function of ξ at the bottom of the plate.

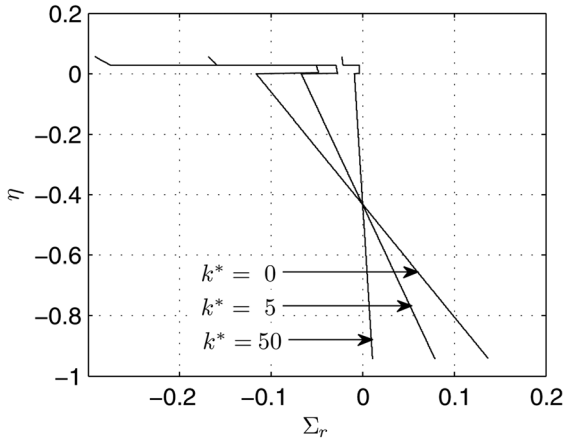

(b) Radial stress as a function of η at the edge of the plate.

Fig. 3 Linear nondimensional stresses for various k^* when the plate is loaded with $P^* = 1$

finely discretized to accurately capture the gradient of the deflection slope.

Substituting the solutions for Θ and U into Eq. (27) gives the nondimensional stresses in the plate due to loading,

$$\begin{Bmatrix} \tilde{\Sigma}_r(\xi,\eta) \\ \tilde{\Sigma}_\theta(\xi,\eta) \end{Bmatrix} = \frac{P^*\Pi(\eta-\eta_{na})}{k^{*2}(1-\nu_n)} \times \begin{Bmatrix} 1+\dfrac{(1-\nu_n)}{(1+\nu_n)}\dfrac{1}{\xi}\dfrac{I_1(k^*\xi)}{I_1(k^*)} - \dfrac{k^*}{(1+\nu_n)}\dfrac{I_0(k^*\xi)}{I_1(k^*)} \\ 1-\dfrac{(1-\nu_n)}{(1+\nu_n)}\dfrac{1}{\xi}\dfrac{I_1(k^*\xi)}{I_1(k^*)} - \dfrac{\nu_n k^*}{(1+\nu_n)}\dfrac{I_0(k^*\xi)}{I_1(k^*)} \end{Bmatrix} \tag{40}$$

The nondimensional stresses as a function of ξ and η are plotted in Fig. 3. The nondimensional stresses exhibit discontinuities across the layers due to discontinuous material properties.

3 Nonlinear Theory

For large deflections, the nonlinear terms in equations Eq. (22) and Eq. (23) become important. The governing equations are discretized and solved using finite difference equations. First, the solution method of Sheplak and Dugundji [4] is followed by introducing a coordinate transformation to concentrate points at the plate's edge where deflection slope gradients are large. The coordinate transformation to a uniformly discretized variable, $\bar{\xi}$, is [11]

Table 2 Non-dimensional parameters

Symbol	Parameter	Value
Λ	Symmetry	0.0162
X	Composite	10.75
η_{na}	N-D Distance to neutral axis	−0.4344
ς	Aspect ratio	0.0072

$$\bar{\xi} = \frac{\ln\left\{\dfrac{\beta+\xi}{\beta-\xi}\right\}}{\ln\left\{\dfrac{\beta+1}{\beta-1}\right\}} \tag{41}$$

where $\beta(>1)$ is the stretching parameter and $\bar{\xi}$ is a set of evenly spaced points. As $\beta \to 1$, the transformation groups more points near $\xi = 1$. After applying the coordinate transformation, the coupled equations become

$$\left(\frac{d\bar{\xi}}{d\xi}\right)^2\frac{d^2\Theta}{d\bar{\xi}^2} + \left(\frac{1}{\xi(\bar{\xi})}\frac{d\bar{\xi}}{d\xi} + \frac{d^2\bar{\xi}}{d\xi^2}\right)\frac{d\Theta}{d\bar{\xi}} - \left(k^{*2} + \frac{1}{\xi(\bar{\xi})^2}\right)\Theta = -P^*\xi(\bar{\xi}) + S_r^*\Theta - \frac{\Lambda}{2}\frac{1}{\xi(\bar{\xi})}\Theta^2 \tag{42}$$

$$\xi(\bar{\xi})^2\left(\frac{d\bar{\xi}}{d\xi}\right)^2\frac{d^2S_r^*}{d\bar{\xi}^2} + \left(3\xi(\bar{\xi})\frac{d\bar{\xi}}{d\xi} + \xi(\bar{\xi})^2\frac{d^2\bar{\xi}}{d\xi^2}\right)\frac{dS_r^*}{d\bar{\xi}} = -\Lambda\left(\begin{array}{l}\xi(\bar{\xi})\left(\dfrac{d\bar{\xi}}{d\xi}\right)^2\dfrac{d^2\Theta}{d\bar{\xi}^2} \\ +\left(\xi(\bar{\xi})\dfrac{d^2\bar{\xi}}{d\xi^2} + \dfrac{d\bar{\xi}}{d\xi}\right)\dfrac{d\Theta}{d\bar{\xi}} - \dfrac{\Theta}{\xi(\bar{\xi})}\end{array}\right) - \frac{X}{2}\Theta^2 \tag{43}$$

and

$$\frac{d^2U}{d\bar{\xi}^2}\left(\frac{\partial\bar{\xi}}{\partial\xi}\right)^2 + \frac{dU}{d\bar{\xi}}\left(\frac{\partial^2\bar{\xi}}{d\xi^2} + \frac{1}{\xi(\bar{\xi})}\frac{\partial\bar{\xi}}{\partial\xi}\right) - \frac{U}{\xi(\bar{\xi})^2} = -\varsigma\left\{\begin{array}{l}\eta_{na}\left(\dfrac{d^2\Theta}{d\bar{\xi}^2}\left(\dfrac{d\bar{\xi}}{d\xi}\right)^2 + \dfrac{d\Theta}{d\bar{\xi}}\left(\dfrac{\partial^2\bar{\xi}}{\partial\xi^2} + \dfrac{1}{\xi(\bar{\xi})}\dfrac{\partial\bar{\xi}}{\partial\xi}\right) - \dfrac{\Theta}{\xi(\bar{\xi})^2}\right) \\ +\Theta\left(\left(1-\dfrac{A_{12}}{A_{11}}\right)\dfrac{\Theta}{2\xi(\bar{\xi})} + \dfrac{d\Theta}{d\bar{\xi}}\dfrac{\partial\bar{\xi}}{\partial\xi}\right)\end{array}\right\} \tag{44}$$

The transformed boundary conditions are

$$\Theta(\bar{\xi}=0) = \Theta(\bar{\xi}=1) = 0 \tag{45}$$

$$\left(\frac{d\bar{\xi}}{d\xi}\frac{dS_r^*}{d\bar{\xi}}\right)_{\bar{\xi}=0} = 0 \tag{46}$$

$$\left(\frac{d\bar{\xi}}{d\xi}\frac{dS_r^*}{d\bar{\xi}}\right)_{\bar{\xi}=1} + \left(1-\frac{A_{12}}{A_{11}}\right)S_r^*|_{\bar{\xi}=1} = -\Lambda\left(\frac{d\bar{\xi}}{d\xi}\frac{d\Theta}{d\bar{\xi}}\right)_{\bar{\xi}=1} \tag{47}$$

and

$$U(\bar{\xi}=1) = U(\bar{\xi}=0) = 0 \tag{48}$$

Second-order finite difference equations are used to discretize Eqs. (42), (43), and (44). Third-order forward and backward

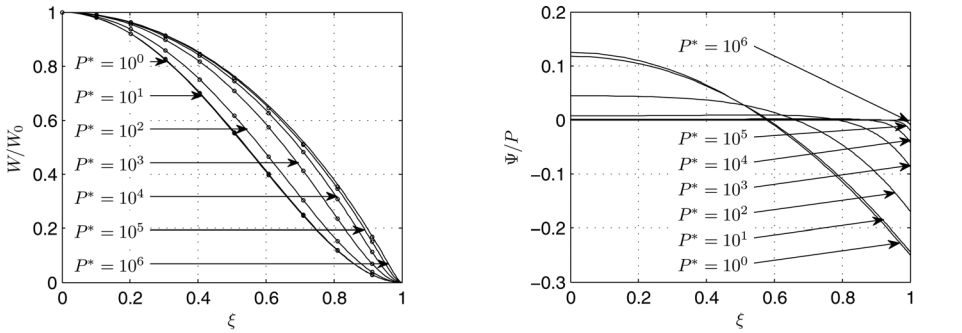

(a) Deflection normalized by center deflection, W_0.

(c) Curvature normalized by P^*.

(b) Deflection slope normalized by center deflection, W_0.

(d) Radial displacement normalized by center deflection, W_0.

Fig. 4 Nonlinear nondimensional solution for various pressure loadings ($k^* = 0$). Finite element results are marked by a circle.

difference equations are used to discretize the boundary conditions. The resulting matrix equations are

$$[\mathbf{F}(\{S_r^*\}, \{\Theta\})]\{\Theta\} = \{J\} \tag{49}$$

$$[\mathbf{K}]\{S_r^*\} = \{L(\{\Theta\})\} \tag{50}$$

and

$$[\mathbf{R}]\{U\} = \{T(\{\Theta\})\} \tag{51}$$

An implicit iterative scheme is used to solve equations, Eqs. (49) and (50). First, Eq. (50) is inverted and solved for $\{S_r^*\}$ given an initial guess for $\{\Theta\}$. Next, $\{S_r^*\}$ and the guess for $\{\Theta\}$ are inserted into $[\mathbf{F}(\{S_r^*\}, \{\Theta\})]$ and Eq. (49). is solved for a new Θ. The new $\{\Theta\}$ is substituted into Eq. (50), and the process is repeated until the solution converges. The initial guess used in this study is the linear solution. The convergence tolerance was set at 0.1% with the stretching parameter $\beta = 1.01$. After a solution is found for $\{\Theta\}$, Eq. (51). is solved for $\{U\}$. Input parameters for the governing equations to solve for $\{\Theta\}$ and $\{S_r^*\}$ are k^*, P^*, Λ, and X. For this paper, Λ and X were kept at constant values given in Table 2 that are indicative of a silicon-silicon oxide-silicon nitride composite [3]. In addition to these values, the nondimensional distance to the neutral axis from the reference axis η_{na} and aspect ratio ς of the plate are needed to solve for the radial displacement, U. Their values are also found in Table 2.

The numerical plate model is validated using the commercial finite element package ABAQUS. An axisymmetric composite plate model meshed with seventy-four 3-node quadratic thin (or thick) shell elements (type SAX2) is used. Residual stress is supplied as an initial condition.

Figure 4 shows the deflection, deflection slope, curvature, and radial displacement for increasing values of P^* (for $k^* = 0$). In the linear solution, the deflection slope and mode shapes are independent of pressure loading. It is interesting to note that as P^* increases, the plate tends to behave similarly to a linear plate with

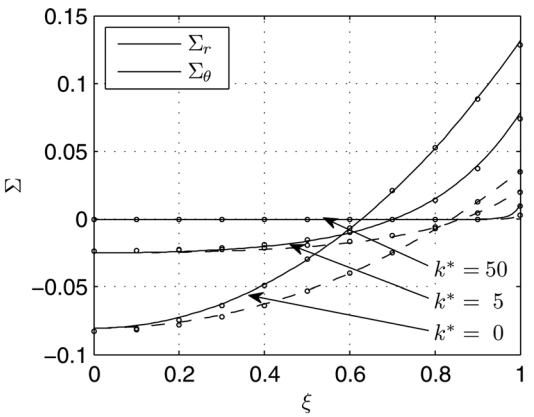

(a) Radial and tangential stress as a function of ξ at the bottom of the plate.

(b) Radial stress as a function of η at the edge of the plate.

Fig. 5 Nonlinear nondimensional stresses for various k^* when the plate is loaded with $P^* = 1$

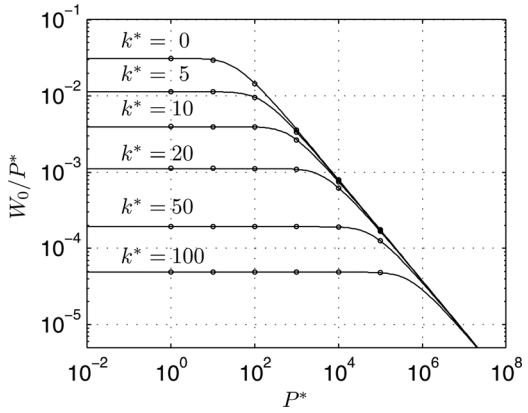

Fig. 6 Mechanical sensitivity versus uniform transverse load for various values of in-plane tension. Finite element results are marked by a circle.

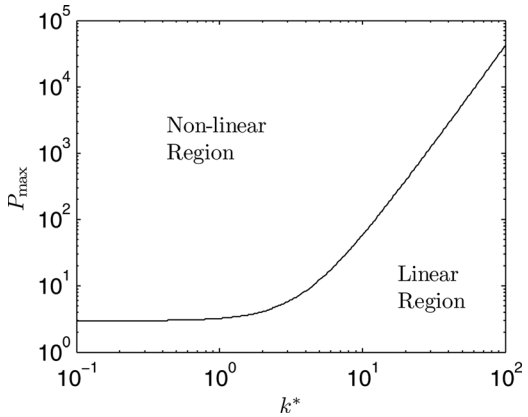

Fig. 7 Maximum transverse loading for linear deflections versus in-plane tension

a large tension parameter [4]. The radial and tangential stresses due to loading are shown in Fig. 5, respectively. Figure 6 shows the transition from linear to nonlinear behavior. The mechanical sensitivity is represented by the center deflection normalized by the transverse load, W_0/P^*. In the linear region, the mechanical sensitivity is constant and independent of the transverse load. This value is also dependent on the composite coefficients, Λ and X. As the transverse load increases, the mechanical sensitivity decreases as the plate stiffens due to nonlinear deflections. When the in-plane tension is increased, the onset of nonlinearity is delayed. In this regime the deflection is independent of Λ and X and the plate transitions to membrane behavior [4]. This can be seen in Fig. 7 where two different composite structures merge to the same solution. The cost of delaying the onset of nonlinearity is a decrease in the linear sensitivity as shown in Fig. 6. Thus, a tradeoff between sensitivity and linearity exists. Figure 7 shows the maximum linear loading for various values of in-plane tension. As the tension parameter k^* increases, the composite plate transitions to membrane behavior and there is no longer dependence on Λ and X.

4 Conclusions

A nonlinear, composite plate model with tensile residual stress has been developed using von Kármán plate theory. The formulation results in two coupled nonlinear equations for the deflection slope and radial force resultant. This paper extends the isotropic plate model of Sheplak and Dugundji [4] to a composite geometry resulting in composite, nondimensional parameters k^* and P^*. This model is verified via the commercial finite element analysis package ABAQUS, and was found to compute the solution $O(10^3)$ times faster. The model captures the tradeoff between mechanical sensitivity and the upper limit of dynamic range. By increasing the in-plane tension of the plate, the upper limit of the dynamic range is increased. This occurs at a detriment to the mechanical sensitivity of the device. This tradeoff must be considered when designing sensors and actuators that incorporate composite plates with tensile stress.

Acknowledgment

This work was supported in part by The Boeing Company. The work of M. Williams and B. Griffin was supported by National Science Foundation Graduate Fellowships.

Nomenclature

$r\{\xi\}$ = radial coordinate (nondimensional)
$z\{\eta\}$ = transverse coordinate (nondimensional)
a = plate radius
h = total plate thickness
z_T, z_B = top and bottom coordinates of the plate
u_r = radial displacement field
u_z = transverse displacement field
u_0 $\{U\}$ = radial displacement at reference plane
w $\{W\}$ = transverse displacement (nondimensional)
$\phi\{\Theta\}$ = deflection slope (nondimensional)
ψ = nondimensional curvature, $d\Theta/d\xi$
ε_r = radial strain
ε_θ = tangential strain
ε_r^0 = radial strain at the reference plane
ε_θ^0 = tangential strain at the reference plane
κ_r = radial curvature term
κ_θ = tangential curvature term
$\sigma_r\{\Sigma_r\}$ = radial stress (nondimensional)
$\sigma_\theta\{\Sigma_\theta\}$ = tangential stress (nondimensional)
σ_0 $\{\Sigma_0\}$ = residual tensile stress (nondimensional)
$[Q]$ = stiffness matrix
$p\{P^*\}$ = uniform transverse load (nondimensional)
Q_r = shear force resultant
$N_r\{S_r^*\}$ = radial force resultant (nondimensional)
N_θ = tangential force resultant
N_0 = residual tensile force resultant
k^* = tension parameter
$\tilde{N}_r$ = incremental radial force resultant
M_r = radial moment resultant
M_θ = tangential moment resultant
M_0 = residual moment resultant
$E\{\Pi\}$ = modulus of elasticity (nondimensional)
ν = poisson's ratio
$[A]$ = extensional stiffness matrix
$[B]$ = flexural-extensional matrix due to coupling
$[D]$ = flexural stiffness matrix
$B_{12}^* = B_{11}A_{12}/A_{11} - B_{12}$
$D^* = D_{11} - B_{11}^2/A_{11}$
$\Lambda = [B_{12}^* h/D^*]$
$\mathrm{X} = \left[\left(A_{11}^2 - A_{12}^2\right)h^2/A_{11}D^*\right]$
ς = aspect ratio, $\frac{h}{a}$
η_{na} = nondimensional distance from the reference axis to the neutral axis, $\frac{B_{11}}{A_{11}}\frac{1}{h}$
$\bar{\xi}$ = transformed nondimensional radial coordinate
β = stretching parameter
$[\mathbf{F}]$ = finite difference coefficient matrix of Θ
$[\mathbf{K}]$ = finite difference coefficient matrix of S_r^*
$[\mathbf{R}]$ = finite difference coefficient matrix of U

References

[1] Brand, O., Hornung, M. R., Baltes, H., and Hafner, C., 1997, "Ultrasound Barrier Microsystem for Object Detection Based on Micromachined Transducer Elements," J. Microelectromech. Syst., **6**(2), pp. 151–160.

[2] Arnold, D. P., Nishida, T., Cattafesta, L. N., and Sheplak, M., 2003, "A Directional Acoustic Array Using Silicon Micromachined Piezoresistive Microphones," J. Acoust. Soc. Am., **113**(1), pp. 289–298.
[3] Homeijer, B., Cattafesta, L. N., Nishida, T., and Sheplak, M., 2007, "Design of a Mems Piezoresistive Microphone for Use in Aeroacoustic Measurements," 13th AIAA/CEAS Aeroacoustics Conference and Exhibit.
[4] Sheplak, M., and Dugundji, J., 1998, "Large Deflections of Clamped Circular Plates Under Initial Tension and Transitions to Membrane Behavior," J. Appl. Mech., **65**, pp. 107–115.
[5] Papila, M., Haftka, R. T., Nishida, T., and Sheplak, M., 2006. "Piezoresistive Microphone Design Pareto Optimization: Tradeoff Between Sensitivity and Noise Floor," J. Microelectromech. Syst., **15**(6), pp. 1632–1643.
[6] Timoshenko, S. P., and Woinowsky-Krieger, S., 1959, *Theory of Plates and Shells*, McGraw-Hill, New York.
[7] Petersen, K. E., 1982, "Silicon as a Mechanical Material," Proc. IEEE, **70**(5), pp. 420–457.
[8] Madou, M. J., 2002, *Fundamentals of Microfabrication: The Science of Miniaturization*, 2nd ed., CRC Press, Boca Raton, FL.
[9] Reddy, J. N., 1999, *Theory and Analysis of Elastic Plates*, Taylor & Francis, London.
[10] Reddy, J. N., 2004, *Mechanics of Laminated Composite Plates and Shells: Theory and Analysis*, CRC Press, Boca Raton, FL.
[11] Tannehill, J. C., Pletcher, R. H., and Anderson, D. A., 1984, *Computational Fluid Mechanics and Heat Transfer*, Hemisphere Publishing Corporation, New York.